IDEM: Iris DEtection on Mobile devices

Maria Frucci
Istituto Calcolo e Reti ad Alte Prestazioni, CNR
Napoli, Italy
maria.frucci@cnr.it

Chiara Galdi
Università di Salerno
Fisciano, Italy
cgaldi@unisa.it

Michele Nappi
Università di Salerno
Fisciano, Italy
mnappi@unisa.it

Daniel Riccio
Università di Napoli, Federico II
Napoli, Italy
daniel.riccio@unina.it

Gabriella Sanniti di Baja
Istituto di Cibernetica E. Caianiello, CNR
Pozzuoli, Napoli, Italy
gabriella.sannitidibaja@cnr.it

***Abstract*— In this paper an iris detection scheme for noisy images acquired by means of mobile devices is presented. Iris segmentation is accomplished by exploiting the use of the watershed transform with the purpose of identifying the iris boundary as much precisely as possible. After a pre-processing step aimed at color/illumination correction, the watershed transform is computed and suitably binarized. Circle fitting is then accomplished to identify the limbus boundary by using curvature approximation and a cost function for circle scoring. The watershed transform is furthermore employed to distinguish, in the zone delimited by the best fitting circle, the regions actually belonging to the iris from those belonging to eyelids and sclera. Finally, pupil detection is accomplished by means of circle fitting and by using a voting function based on homogeneity and separability criteria. The suggested iris detection scheme has a positive impact on an the accuracy in computing the iris code, which has in turn a positive impact on the performance of iris recognition.**

Keywords—iris detection; watershed transformation; circle fitting; smart mobile devices.

I. INTRODUCTION

Iris recognition is commonly used in security applications, e.g., physical access control, computer log-in, international border crossing, and national ID cards, due to the non invasiveness of the available iris acquisition devices, which are based on near infrared or visible light technology, and being characterized by a large number of features, e.g., uniqueness, external visibility and life stability, that make the performance of iris recognition higher with respect to that of other biometrics. A rich literature covering the key subjects in the context of iris recognition is available [1-5].

The iris is the annular part of the eye delimited by the white sclera and surrounding the pupil, which is generally the darkest part of the eye image. Iris features structure is so rich that the probability of finding two individuals with the same iris features structure is almost zero [1]. Thus, under good illumination acquisition conditions and with a cooperative subject, iris recognition can be achieved by using simple image processing tools. However, the effectiveness of iris recognition accomplished under controlled acquisition conditions significantly decays when iris has to be captured from moving subjects, under uneven lighting conditions and by means of rapidly spreading new ICT acquisition tools, such as smart mobile devices.

An iris recognition system has to accomplish a number of tasks: 1) eye image acquisition, 2) iris segmentation, 3) normalization, 4) iris coding and 5) recognition. Of course, all these tasks have to be done accurately, but accuracy is really crucial as regards iris segmentation, since the quality of the result of this task strongly conditions the outcome of the whole recognition process. In this paper we focus on iris segmentation for eye images taken by means of smart mobile devices. In particular, we describe an iris segmentation method based on the use of the watershed transformation, and show that it identifies more precisely the iris boundary and, hence, allows us to obtain a more accurately computed code. Our technique for Iris Detection on Mobile devices (IDEM) is derived from a technique that we have recently introduced [6,7]. IDEM is based on the use of the watershed transformation that identifies more precisely the iris boundary and, hence, allows us to obtain a more stable iris code. IDEM is tested on a set of 1500 eye images of 75 individuals. Images have been acquired, outdoor and indoor, by using different mobile devices, specifically a tablet Samsung Galaxy, an Apple iPhone 5 and a Samsung Galaxy S4 smartphone. Due to the different technical features of the adopted cameras and to the uncontrolled acquisition conditions, at least as regards illumination and distance, the images obtained for the same individual are quite different from each other. Our aim is to show that this notwithstanding IDEM is able to reliably detect the irises so that recognition can be accomplished in a satisfactory manner. The interoperability of IDEM is also investigated by performing cross-datasets experiments. IDEM includes a pre-processing phase, described in Section II, to improve the quality of the input eye image. Section III is concerned with computation and binarization of the watershed transform of the gradient image, which will

1051-4651/14 $31.00 © 2014 IEEE
DOI 10.1109/ICPR.2014.308

facilitate circle fitting. Section IV describes in detail how IDEM performs iris detection. This is accomplished by employing twice circle fitting. The first time, circle fitting is done to detect limbus boundary. IDEM furthermore exploits the use of the watershed transform to distinguish among the pixels inside the circle better fitting the limbus boundary those really belonging to the iris from those possibly belonging to eyelids and sclera. Then, circle fitting is done for pupil detection. A short description of the iris recognition approach used to test recognition accuracy and interoperability is provided in Section V. Section VI regards the experimental setup, while final remarks are given in Section VII.

II. PREPROCESSING

IDEM works with images in the RGB color space. Each color is a point in the 3D Cartesian space with red, green and blue as coordinate axes. Since the R, G, B values are in the range [0,255], colors are the points within a cube spanning from the origin (0, 0, 0), black, to (255, 255, 255), white.

A color/illumination correction is accomplished to reduce local distortions introduced during the uncontrolled iris acquisition, such as shadows and different color temperature. To this aim, the three RGB components are processed separately as gray level images by a Gaussian filter, with experimentally fixed kernel dimension n=128 and variance σ=10. Then, we take into account that, according to the Lambertian reflectance theory, the image intensity of the diffusely reflected light is obtained by multiplying the albedo by the intensity of the incoming light and that the albedo can be computed as the ratio, pixel by pixel, between the intensity image and its smoothed version filtered by a Gaussian filter. Thus, for each of the three gray level images we build a new image whose pixels are set to the ratio between the values of the homologous pixels in the gray level image and in its filtered version. The values are normalized in the range [0,1] and mapped again in [0, 255]. The three modified gray level images are then combined to originate the color/illumination corrected image. As an example, refer to Fig. 1 showing to the left the original image and in the middle the color/illumination corrected image.

Size reduction and smoothing is then accomplished to limit the total computation time and to reduce the noise in the eye images. Size reduction to 200×150 pixels is obtained by using a linear interpolation method to compute the three color coordinates of each pixel p in the reduced size image as the arithmetic mean of the corresponding coordinates of the pixels in the block of the original image associated to p. Smoothing is done by using a median filter with window size 7×7. See Fig. 1 right.

Fig. 1. From left to right: an eye image, the image resulting after color/illumination correction, and the resized and smoothed image.

III. WATERSHED TRANSFORM AND BINARIZATION

The watershed transformation divides an image into a number of disjoint regions, where pixels in the same region are characterized by a certain degree of homogeneity while pixels in adjacent regions are not. Image partition is obtained by applying region growing to a suitable set of seeds, generally detected as the regional minima in the gradient image. Two approaches, known as watershed transform by immersion and watershed transform by topographical distance, have been suggested in the literature [8].

The 3×3 Sobel edge filter is applied to each of the three color components. The gradient image of the color eye image is obtained as the average of the three computed images. See Fig. 2 left. Actually, an edge enhancing process - termed Lower Completion in [8] - is also applied to each of the three computed images before combining them to get the gradient image. The effect of Lower Completion can be seen in Fig. 2 middle-left. Regional minima are detected in the gradient image and the topographical distance approach [8] is followed to generate the watershed transform W (Fig. 2 middle-right).

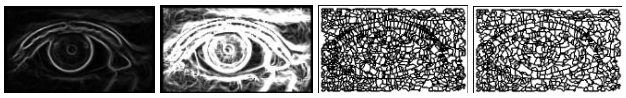

Fig. 2. From left to right: gradient image, edge enhancement due to Lower Completion, the watershed transform, the simplified watershed transform after region merging.

Each partition region is associated a unique representative color, computed as the mean value of the colors of pixels belonging to it. To simplify the structure of W, we perform merging of adjacent regions, provided that their colors differ less than a threshold δ (experimentally set to 50). The watershed lines resulting after merging are shown in Fig. 2 right.

For each region R_i, let db_i and dw_i be the Euclidean distances of its representative color c_i (r_i, g_i, b_i) from black (0,0,0) and white (255,255,255). Moreover, let db and dw be the arithmetic means of the distances from black and white respectively computed for all the representative colors. Finally, let dbw be the distance between black and white. Since in general pupil and iris (sclera and eyelids) have colors closer to black (white) than to white (black), a comparison of c_i with db and dw could be used to decide whether R_i should be ascribed to the foreground (i.e., R_i can be tentatively regarded as belonging to iris or pupil), or to the background (i.e., R_i can be tentatively regarded as belonging to eyelids or sclera). If it is both $db_i > db$ and $dw_i > dw$, a decision on the assignment of R_i cannot be taken, while if it is $db_i \le db$ and $dw_i \le dw$ R_i could be assigned to both the foreground and the background. In other words, there are cases in which some regions may remain unassigned (which happens if it results $db+dw<dbw$), and cases where assignment could be done in an ambiguous manner (which happens if it results $db+dw \ge dbw$). Thus, db and dw, though should be reasonably involved in the binarization process, cannot be used directly as thresholds. We use the ratio $dbw/(db+dw)$ as a multiplicative weight for the

arithmetic mean *db* and define the threshold T for a preliminary segmentation of W as as $T=db\times dbw/(db+dw)$. Regions whose representative color has a distance from black smaller than (larger than or equal to) T are tentatively assigned to the foreground (background). Binarization is then refined by taking into account the representative colors of the regions tentatively assigned to the foreground as well as average foreground color, c_F, and average background color, c_B, respectively. The colors c_F and c_B are computed as the arithmetic means of the colors of the pixels belonging to regions that have been tentatively assigned to the foreground and to the background, respectively. Any region R_i tentatively assigned to the foreground and such that the distance between c_i and c_B is not larger than the distance between c_i and c_F is eventually assigned to the background.

IV. Iris Detection

Since the regions of W consist of pixels characterized by a certain homogeneity as far as color is concerned, from now on we refer to a quantized version of the true color input image, where the colors of pixels in the same region are replaced by the representative color for that region (see Fig. 3 left).

To detect the limbus boundary we use the image B, binarized version of W, compute the contour of the foreground as the set of black pixels having at least a 4-adjacent white pixel (see Fig. 3 middle-left) and apply to it the circle detection procedure [9].

Since the foreground of B does not exclusively include iris and pupil, before applying circle fitting we analyze the curvature along the extracted contour so as to divide it into components along which the curvature is very smooth (parts of the contour shown in yellow in Fig. 3 middle-right), which are linked by contour components characterized by strong curvature changes (parts of the contour shown in blue in Fig. 3 middle-right). Circle fitting will be accomplished only on the contour components that are smooth curves and include a sufficiently large number of pixels (at least 150 pixels in our work). For the sake of completeness, we remark that to save computation time, we use an estimate of curvature, rather than calculating the exact value. Actually, while tracing a contour component, its pixels $p_1,p_2,\ldots,p_n$ are recorded in a list. For each point p_i, the point p_{i+t} is considered, where t is fixed by taking into account the length L of the contour as $t=4\times\lfloor log_2(|L|)\rfloor$. The curvature at p_i is estimated by the distance between the mid point of the straight line segment joining p_i and p_{i+t} and the contour point midway along the contour arc delimited by p_i and p_{i+t}.

Among all circles detected by the algorithm [9] as fitting the selected smooth components of the contour, those included for at least 80% in the image undergo a voting process to detect the best fitting circle. The score for a given circle C, centered in (x, y) and with radius r, is computed by considering two additional circles centered in (x, y) and with radii $0.9r$ and $1.1r$, respectively. For each point in C, represented in the polar coordinate system (ρ,θ), the two pixels located at the same angle θ, on the two circles with radii $0.9r$ and $1.1r$ are considered and the total sum of differences between their corresponding two pixels in the binary image (Fig.3 left) is taken as score for C. The circle with the maximal score, shown in red in Fig. 3 right, is taken as the one better fitting the limbus boundary.

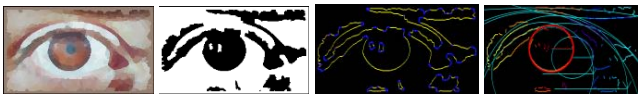

Fig. 3. From left to right: the quantized image where all pixels in the same region of the watershed transform are assigned the representative color of that region, the binarized watershed transform, contour components with smooth curvature (yellow parts) and strong curvature changes (blue parts), the best fitting circle (in red).

We use again the watershed transform W and its binarized version B to correctly identify, among the pixels enclosed by the circle better fitting the limbus, the pixels actually belonging to iris and pupil. To this purpose we take into account all the regions of the W at least partially overlapping the detected circle (shown in purple in Fig. 4 left). Regions of W totally overlapping the circle may belong to the foreground of B (shown in red in Fig. 4 middle-left) or to the background of B (shown in blue in Fig. 4 middle-left). Regions of W only partially overlapping the circle (shown in yellow in Fig. 4 middle-left) may belong to the foreground or the background of B.

Fig. 4. From left to right: circle detected by circle fitting (purple) superimposed on the watershed transform, watershed regions totally overlapping the circle (red and blue) and partially overlapping the circle (yellow), result after the assignment to the foreground (black) of totally overlapping regions, subdivision of the partially overlapping regions.

Let c_{iris} be the arithmetic mean of the colors of the pixels of the quantized image that: i) are within the circle and ii) are in the foreground of B. Only the regions in red and part of the regions in yellow in Fig. 4 middle-left contribute to c_{iris}. Moreover, let c_{back} be the arithmetic mean of the colors of the pixels of the quantized image that are outside the circle and that have been assigned to the background in B. Note that the regions in blue in Fig. 4 middle-left do not contribute to c_{back}. The values c_{iris} and c_{back} can be seen as the colors representing iris and pupil, and the background respectively.

To achieve the desired segmentation of W, where the foreground includes only iris and pupil, we will assign to each region of W one out of two markers, f and b. We can safely assign the background marker b to the watershed regions that do not overlap at all the circle. In fact, these regions certainly belong to the background. As for the remaining watershed regions, some further processing is necessary to decide on their assignment. To this aim, we introduce two preliminary markers, $f+$ and $f-$, and assign them to the watershed regions completely overlapping the circle (marker $f+$, red and blue regions in Fig. 4 middle-left) and only partially overlapping the circle (marker $f-$, yellow regions in Fig. 4 middle-left).

Any region R_i with marker *f*+ has its marker changed into *f* if at least one of the following conditions is satisfied:

1) the Euclidean distance between c_i and c_{back} is larger than the Euclidean distance between c_i and c_{iris};

2) R_i belongs to the foreground in B, and at least one of its neighboring regions$_i$ has marker *f*+, while no neighboring regions exist with marker *f*-.

The first condition segments as belonging to the foreground any watershed region whose representative color is closer to the average color of iris and pupil, than to the the average color of the background. The second condition takes into account also the classification of the watershed regions in the binarized image B, to assign to the foreground regions that, though characterized by a representative color that would justify assignment to the background, are not isolated as regards the property of being completely overlapping the circle, and have been assigned to the foreground in B.

Since regions with marker *f*+ may still exist, a second process is done, which is based on the minimum Euclidean distance d_{min} between the representative color of a region with marker *f*+ and the representative colors of its adjacent regions that have already been assigned to the foreground. If the Euclidean distance between the representative color of the region at hand and c_{back} is not smaller than d_{min}, the marker is changed to *f*. Otherwise, the marker is set to *b*.

The rationale for assigning to the foreground a region whose representative color is closer to the average color of the background than to the average color of the iris, is that some neighboring regions, already assigned to the foreground, exist to which the color of the region at hand is closer than to the average color of the background.

The regions having initially marker *f*+ and assigned to the foreground (background) are shown in black (white) in Fig. 4 middle-right. As for the regions with initial marker *f*-, they are divided into two sub-regions, respectively including pixels within the circle, and pixels outside the circle. The former sub-regions (shown in red in Fig. 4 middle-right) receive marker *f*+ and the latter sub-regions (shown in green in Fig. 4 middle-right) receive marker *b*. Then, the quantized image and the values c_{iris} and c_{back} are updated before the final decision is taken for the new regions with marker *f*+. Any such a region R_i is assigned to the foreground if at least one of its neighboring regions has already been assigned to the foreground, and at least one of the following conditions is satisfied:

i) the Euclidean distance between c_i and c_{iris} is not larger than the Euclidean distance between c_i and c_{back}

ii) the Euclidean distance between c_i and c_{back} is not smaller than the minimum Euclidean distance in color between c_i and the regions adjacent to R_i and with marker *f*.

Otherwise, the region R_i with marker *f*+ is assigned to the background. The detected foreground is shown in Fig. 4 right.

Since pupil is always inside the iris, only the portion of the color/illumination corrected image inside the circle approximating the limbus is considered as the Region Of Interest (ROI) for pupil detection. The color ROI image is converted to a gray level image that is processed by Canny filter. Ten different thresholds {0.05, 0.10, 0.15, ..., 0.55} are used, which originate ten Canny filtered images. In each of them, the connected components of edge pixels are extracted and pixel counting is performed. Circle fitting [9] is accomplished for the connected components including enough pixels (more than 50 pixels in our work). Only circles entirely included in the circle approximating the limbus processed by a voting function based on homogeneity and separability. Homogeneity is evaluated in terms of the histogram of the region included by the circle. Separability is evaluated by an operator similar to the Daugman's integrodifferential operator that averages, over all angle θ, the difference in grey levels of corresponding pixels on two circles concentric with the candidate circle with radius ρ, and having radii ρ_1=0.9ρ, and the ρ_2=1.1ρ. The score assigned to each circle is the sum of the scores on homogeneity and on separability. The circle with the maximal score is selected as the one better approximating the pupil.

A few examples showing the performance of our iris detection algorithm can be appreciated in Fig. 5, where red and green curves delimit the limbus boundary and the pupil boundary, respectively.

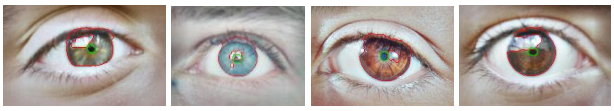

Fig. 5. Red and green curves denote the limbus and pupil boundaries detected by IDEM.

V. IRIS RECOGNITION

Since this paper also aims to evaluate the interoperability of IDEM among different mobile devices, an iris recognition approach has been exploited for this purpose. After the detection process, the iris is extracted from the whole image and the original annular region in the Cartesian space is mapped to a rectangular region in the polar space by applying the rubber sheet model suggested by Daugman [1]. A color space conversion from the original RGB to the HSV is performed to treat the luminance and chrominance information separately. A color histogram of 64 bins is built by combining information coming from the H and S channels, while the cumulative sums approach (CSUM) [10] is applied to the luminance channel V to extract a binary iris code. Even when comparing two irises, histograms and binary codes are treated separately. The cosine dissimilarity is used for the former, while the Hamming distance is adopted for the latter, and the two resulting distance values are then combined by means of the simple sum rule.

VI. EXPERIMENTAL RESULTS

The images IDEM has been tested on are from the MICHE iris database [12]. The MICHE dataset consists of 3132 iris

images, either left or right, captured from 75 subjects by means of three different mobile devices: i) a Samsung Galaxy S4 (SG4), ii) an iPhone 5(IP5) and a Samsung Galaxy Tablet (SGT). For the SG4 and the IP5 devices the iris images have been acquired from both the frontal and the retro camera, while only the frontal camera acquisition is available for SGT, as it is not equipped with a retro camera. All the images have been acquired during the same session both in indoor and outdoor settings, so that each subject is provided with at least 40 pictures (4 for each of the 10 modalities - indoor/outdoor, frontal/retro, different device). In our experiments we considered only a subset of the whole MICHE, which consists of 1500 images that are the first two pictures of all 75 subjects in the 10 acquisition modalities. Iris images were manually segmented to extract binary masks that should be accepted as ground truth in order to compare the performance of IDEM with respect to that of a state of the art approach, namely ISIS [2].

The accuracy of segmentation provided by both tested algorithms is quantitatively evaluated in terms of the percentage of errors measured in pixels. For the latter, circle fitting is applied to binary masks to approximate both iris and pupil circles separately. The discrepancy in pixel between parameters of the circles computed by the testing algorithm and those provided by the ground truth are normalized according to the image resolution and multiplied by 100. The errors percentage is computed as the average of the errors over all images in the testing dataset. It came out from the experiments that for a completely inaccurate detection the errors percentage is generally higher than a given threshold ε_{out}, that is directly proportional to the median value m_d computed over all the errors in the subset of tested images ($\varepsilon_{out}=8 \cdot m_d$). These cases can be considered as outliers and have a negative effect on the performance evaluation. For this reason, in all tables results are reported for both cases, in which the outliers have been included or not in the computation. Furthermore, the percentage of outliers, by itself, can be seen as an additional parameter to assess the effectiveness of a segmentation approach. In each recognition test, two images per subject have been considered, one for the enrollment (gallery) and the other for testing (probe), while the segmentation accuracy was computed on the subset built as the union of both gallery and probe.

The aim of the first experiment was to assess the performance of IDEM both in terms of segmentation and recognition accuracy with respect to that provided by ISIS. The accuracy is evaluated in terms of decidability [12]. The decidability measures the performance of a recognition system by evaluating the average of scores it provides for genuine and impostor users. All images are acquired indoor with the retro camera (high resolution) for SG4 and IP5 and the frontal camera for the SGT. In this experiment probe and gallery sets are always composed of images acquired by the same mobile device. Results are reported in Table 1 and Table 2. Results in Table 1 underline three main aspects: i) IDEM outperforms ISIS on low resolution images; ii) IDEM performs better in locating the iris than the pupil; iii) IDEM produces a lower number of outliers and the increment in accuracy is larger than that observed for ISIS when the outliers are not included in the performance evaluation. The higher robustness of IDEM on low quality images can be explained by the nature itself of the segmentation process. Indeed, IDEM first locates iris and then limit the search for the pupil in the region delimited by the limbus. ISIS performs in the opposite way by first searching for the pupil and then polarizing the image with respect to the pupil center. However, in low resolution images the pupil area is very small, making a precise localization of its center a difficult task and this jeopardize all the subsequent steps performed by ISIS. On the contrary, the iris still remains distinguishable even when the quality of the input image is low, thus allowing IDEM to better locate it. This also explains why IDEM provides a higher accuracy for iris parameters than for those corresponding to the pupil as mentioned by the observation (ii).

Table 1. Segmentation accuracy measured in terms of percentage of error with respect to manual segmentation for the two tested approaches (ISIS and IDEM) on probe/gallery images acquired by the same mobile device.

Device	Method		Iris CX	Iris CY	Iris Rad.	Pupil Cx	Pupil CY	Pupil Rad.
IP5	ISIS out 30%	out	2.40	3.18	4.00	2.27	2.39	1.52
		nout	0.67	1.78	1.23	0.34	0.66	0.35
	IDEM out 24%	out	3.63	**3.11**	**1.26**	3.63	**2.08**	**0.60**
		nout	**0.44**	**1.18**	**0.52**	0.37	0.81	0.40
SG4	ISIS out 27%	out	3.16	3.71	3.15	1.14	1.13	1.20
		nout	0.51	1.53	1.02	0.36	0.62	0.41
	IDEM out 29%	out	3.65	4.42	**1.53**	3.70	4.42	**0.65**
		nout	**0.357**	**1.47**	**0.62**	0.46	1.27	**0.37**
SGT	ISIS out 50%	out	5.90	7.71	10.08	5.88	7.58	5.39
		nout	3.00	5.57	4.07	3.03	5.41	1.77
	IDEM out 28%	out	6.43	**5.55**	**2.38**	6.62	**5.72**	**1.14**
		nout	**1.43**	**2.60**	**1.31**	**1.63**	**2.82**	**0.83**

Regarding the number of outliers, both ISIS and IDEM fail in locating iris/pupil, because some images into the dataset are affected by large occlusions (half-closed eyes) or severe illumination changes and out of focus conditions. Generally, these kinds of distortions often occur, since the mobile device is hold in people hands during the acquisition process.

Table 2. Recognition accuracy measured in terms of decidability for the two tested approaches (ISIS and IDEM) on probe/gallery images acquired by the same mobile device.

Method	Device		
	IP5	SG4	SGT
ISIS	0.474	0.705	0.694
IDEM	**1.039**	**0.799**	**0.870**

It is worth to notice from Table 2 that IDEM always induce a higher decidability value, when combined with the implemented iris recognition algorithm (described in Section V). This can be ascribed to the fact that despite some cases in

which IDEM is worse or more often comparable to ISIS, in average it is able to provide a more accurate segmented iris. Given that IDEM has shown its superiority in terms of both segmentation precision and recognition accuracy with respect to ISIS, the latter was not further considered in the following experiments.

In the second experiment, the interoperability of the IDEM approach was evaluated, since probe and gallery sets were acquired with different mobile devices. Results for this experiment are reported in Table 3.

Table 3. Recognition accuracy measured in terms of decidability for the IDEM approach on probe/gallery images acquired by different mobile devices.

IDEM		Gallery		
		IP5	**SG4**	**SGT**
Probe	**IP5**	0.474	0.584	0.144
	SG4	0.0892	0.799	0.887
	SGT	0.225	0.243	0.870

By visually inspecting images acquired by different devices, it comes evident the discrepancy in image quality among pictures captured by the IP5 device and those obtained by the SG4 and SGT. Indeed, the former shows a higher quality than the latter two for both frontal and retro camera. This difference in image quality mainly motivates the poor performances obtained by IDEM when tested on cross-datasets: the probe (gallery) acquired by the IP5 and the gallery (probe) by a different device (SG4 or SGT). This is further confirmed by the higher decidability values obtained by IDEM when cross-testing is performed on images acquired in turn by the SG4 and SGT devices.

In the last experiment the recognition performance of IDEM was assessed by holding indoor images into the gallery and the outdoor images into the probe. This scenario is more plausible than the opposite one, as it can be supposed that the enrollment of a person is rarely performed (may be just the first time), and then it is likely carried out in controlled settings. On the contrary, testing is very frequent and may be often performed in an uncontrolled environment. Numerical results for this experiment are shown in Table 4.

Table 4. Recognition accuracy measured in terms of decidability for the IDEM approach on probe/gallery images acquired by different mobile devices.

Method	Device		
	IP5	**SG4**	**SGT**
IDEM	**0.44**	**0.46**	**0.42**

Observing values in Table 4, it comes out that there is no appreciable difference regarding the decidability obtained for all the devices. This underlines that the image resolution offered by new technology like IP5 and SG4 even if higher than that provided by older devices like the SGT, is not able alone to compensate for large distortions affecting iris images when acquired in a completely uncontrolled setting, making iris recognition on mobile devices a more challenging task than that addressed when dealing with other biometric traits like face.

VII. Conclusion and Future Work

In this paper we introduced a new iris segmentation technique for mobile devices, namely IDEM. It exploits the watershed transform in a twofold manner, to binarize the iris image and to refine the foreground/background segmentation. Curvature analysis and circle fitting are then involved to precisely locate iris and pupil. IDEM also implements a color based recognition technique performing iris matching in the HSV color space. This approach has been tested on the MICHE dataset, in order to assess its performances in terms of segmentation precision, recognition accuracy and interoperability. Results have shown that, in average, it outperforms other techniques from the state of the art, regardless of which of the three mobile devices used in our experiments is considered. Several tests have been conducted with respect to indoor/outdoor acquisition settings and cross-datasets. Results have shown that iris detection/recognition on mobile device is a challenging task, but also underlined the high potential of the proposed technique.

References

[1] J.G. Daugman, High confidence visual recognition of persons by a test of statistical independence, IEEE Transactions on Pattern Analysys Machine Intelligence, vol. 11, no. 15, pp. 1148–1161, 1993.

[2] M. De Marsico, M. Nappi, D. Riccio, IS_IS: Iris Segmentation for Identification Systems, *Proceedings of the International Conference on Pattern Recognition (ICPR 2010)*, pp. 2857-2860, 2010.

[3] M. Burge, K. W. Bowyer, in Handbook of Iris Recognition, London, UK, 2013.K. Siddiqi and S.M. Pizer, Eds., "Medial Representations: Mathematics," Algorithms and Applications, Springer, 2008.

[4] K.W. Bowyer, K.P. Hollingsworth, P.J. Flynn, Image understanding for iris biometrics: a survey, Computer Vision Image Understanding, vol. 110, no. 2, pp. 281–307, 2008.

[5] K.W. Bowyer, K. P. Hollingsworth, P.J. Flynn, A Survey of Iris Biometrics Research: 2008-2010, in Handbook of Iris Recognition, M. Burge and K. W. Bowyer, eds., Springer, Chapter 2, pp. 15-54, 2013.

[6] M. Frucci, M. Nappi, D. Riccio, Gabriella Sanniti di Baja, Using the Watershed Transform for Iris Detection, Proceedings of the International Conference on Image Analysis and Processing (ICIAP 2013), pp. 269-278, 2013.

[7] M. Frucci, M. Nappi, D. Riccio, Watershed Based Iris SEgmentation, Proceedings of the 5th Mexican Conference on Pattern Recognition (MCPR 2013), pp. 204-212, 2013.

[8] J.B.T.M. Roerdink, A. Meijster, The watershed transform: definitions, algorithms and parallelization strategies, *Fundamenta Informaticae*, vol.41, no.1-2, pp. 187-228, 2001.

[9] G. Taubin, Estimation of planar curves, surfaces and nonplanar space curves defined by implicit equations, with applications to edge and range image segmentation, *IEEE Transactions on Pattern Analysys Machine Intelli*gence, vol. 13, no. 13, pp. 1115-1138, 1991.

[10] E. Raj, M. Chirchi, R.D. Kharadkar, Biometric Iris Recognition for Person Identification using Cumulative Sum Algorithm, *International Journal of Scientific & Engineering Research*, vol. 3, no. 5, May 2012.

[11] J.B.T.M. Roerdink, A. Meijster, The watershed transform: definitions, algorithms and parallelization strategies, *Fundamenta Informaticae*, vol.41, no.1-2, pp. 187-228, 2001.

[12] http://biplab.unisa.it/MICHE/databas